AIAA JOURNAL
Vol. 35, No. 2, February 1997

Raasch Challenge for Shell Elements

N. F. Knight Jr.*
Old Dominion University, Norfolk, Virginia 23529-0247

The Raasch challenge problem of a curved strip with a tip in-plane shear load is examined in an attempt to better understand how certain shell element features affect its solution. Various shell element formulations are used in the assessment in an attempt to define any inherent pathological problems of the shell finite elements or the problem itself. Six different flat shell elements and two solid brick elements are assessed by this problem, and the findings are very surprising. Selected aspects of shell finite-element development that are relevant to this problem are briefly described. These aspects are the inclusion of transverse shear flexibility in the element formulation, the addition of drilling degrees of freedom, and the realignment of shell surface normals. Shell elements without transverse shear flexibility appear to converge to an appropriate value (i.e., 5% stiffer than the three-dimensional solution). Shell elements with transverse shear flexibility do not appear to converge.

Introduction

THE quality and performance of shell finite elements has been the subject of study for users and developers of finite element software systems for many years (e.g., see Refs. 1 and 2). Often large-scale simulations of a complex system yield results that are perhaps just a little peculiar to the analyst. This usually prompts the analyst to scrutinize the computed solution in detail, and frequently at least minor modifications are made to the finite element model. On some occasions, such modifications cause a completely unexpected numerical result. However, because the structural system and finite element model are quite complex, such an anomaly is often attributed to possible errors in making the modeling changes, which in turn may possibly be affecting other aspects of the finite element model (e.g., fastener modeling, multi-point constraints). This is true in many cases, but, in other cases, a problem associated with the finite elements themselves is masked by the overall complexity of the simulation being considered.

Problems that appear to be very simple are usually deceptively simple (e.g., see Ref. 3). These problems are often designed to test inherent features of the elements, and even though by themselves these problems appear to be only of academic interest, such geometries and loading conditions are commonly found in actual large-scale structural models. The insight gained by examining the performance of a particular element by a gauntlet of test cases can be of considerable use to an analyst trying to verify and establish the reliability of a given finite element model. The standard set of test problems posed by MacNeal and Harder[3] is a good example of such problems for linear elastic analysis. Many finite element developers now use the MacNeal–Harder test problems as a standard suite of problems to test and grade element performance. This set of problems involves mostly flat geometries and focuses heavily on determining the influence of severe element distortion on element performance as measured by normalized values of deflections. Belytschko and Liu[4] posed three shell test problems, including the pinched cylinder problem, as part of an obstacle course to screen out elements with either shear or membrane locking. Accuracy of stresses is not considered in these problems. These problems include only three shell problems—none of which sufficiently tests an element's performance in a bending–twisting-type deformation mode.

This paper deals with a curved strip problem posed in 1990 by Ingo Raasch of BMW in Germany—the Raasch challenge.[5,6] Various shell element formulations are used in this assessment in an attempt to define any inherent pathological problems of the shell finite elements or the problem itself. Six different flat shell elements and two solid brick elements are assessed by this problem, and the findings are very surprising. The paper first briefly describes selected aspects of shell finite element development that are relevant to this problem. Among these aspects are the inclusion of transverse shear flexibility in the element formulation, the addition of drilling degrees of freedom, and the realignment of shell surface normals. Next, the computational framework used for this study is described, followed by a description of the Raasch challenge problem. Numerical results and discussion are then presented.

Received Feb. 9, 1996; presented as Paper 96-1369 at the AIAA/ASME/ASCE/AHS/ASC 37th Structures, Structural Dynamics, and Materials Conference, Salt Lake City, UT, April 15–17, 1996; revision received July 18, 1996; accepted for publication Nov. 18, 1996; also published in *AIAA Journal on Disc*, Volume 2, Number 2.

*Professor, Department of Aerospace Engineering. Associate Fellow AIAA.

Shell Finite Element Development

Shell finite element development continues to be an active area of research even though some have commented that everything is done in finite element development. Although significant advances have been made and complex structural systems have been designed and built by today's shell element technology, there still remain unanswered questions and pathological problems associated with many elements.[4,7] The need for increased reliability in our computed solutions continues to grow as the reliance on analytical results increases for systems in which verification by experiment is not feasible, economical, or timely. Aspects of shell element development discussed in this paper include transverse shear flexibility, drilling freedoms, and surface normals.

Transverse Shear Flexibility

Early plate and shell element formulations were based on the Kirchhoff assumptions, which neglected the effects of transverse shear deformations. Such formulations led to the development of conforming and nonconforming elements with a C^1 continuity requirement on the interpolation functions for the nodal degrees of freedom. Once the effects of transverse shear deformations are included in the element formulation, the continuity requirement is reduced to being only C^0 continuous along interelement boundaries. For the most part, first-order, shear-deformation theory is used, which is applicable to moderately thick structures (i.e., when the ratio of the smallest planar dimension of the structure to its thickness is approximately equal to 10). Thick structures (i.e., when this ratio is less than 10) require either a higher-order plate theory or a three-dimensional analysis. The analysis of very thin structures (i.e., when this ratio is much greater than 10) may exhibit locking within an element for some formulations (e.g., see Ref. 1).

Drilling Freedoms

Drilling degrees of freedom (or simply drilling freedoms) are defined as the rotational degrees of freedom normal to the plane of the element. In most cases, this drilling freedom is the sixth nodal degree of freedom and usually is denoted by θ_z (assuming that the surface normal is in the local z direction). This freedom

is not represented in the membrane kinematics of the shell and, as such, does not provide any corresponding structural stiffness if not included in the finite element approximations. Two basic approaches have been widely implemented: 1) use of artificial drilling stiffness parameter to remove rank deficiency for those elements without drilling freedoms and 2) inclusion of drilling freedoms in the finite element membrane approximations.

Finite element models based on elements without this drilling freedom at the element level may in fact have drilling degrees of freedom at the global or assembled structural level. In some cases, an artificial drilling stiffness parameter is used to avoid the singularity associated with this freedom. This artificial stiffness parameter acts as a spring stiffness for the sixth degree of freedom and is prescribed by the user. The value specified for this stiffness parameter may dramatically affect the solution if given an inappropriate value. One approach is to specify a large value for this parameter; hence, it acts as a penalty parameter and forces the computed solution for the drilling degrees of freedom to be nearly zero. Here, each nodal point must be examined by the analyst to determine whether to impose the penalty. For example, along the skin-stiffener intersection of a branched shell model of a blade-stiffened panel, the drilling freedoms of the elements in the blade stiffener are bending rotations of the elements in the panel skin, and the penalty is not needed. For built-up shell structures, adding artificial drilling stiffness at nodes on elements that intersect at moderately large angles should not be done. However, if the elements are coplanar, then the penalty is required to avoid the singularity associated with this drilling freedom. Alternatively, a very small value may be specified for the artificial drilling stiffness parameter, and hence the contribution to the total strain energy will be nearly zero regardless of the computed solution for the drilling degrees of freedom. Here, each and every nodal point can be assigned this value initially, and if during assembly of the finite element stiffness matrix some bending stiffness is added to those degrees of freedom, the penalty is essentially removed. This artificial stiffness parameter approach does address the singularity or rank deficiency of the stiffness matrix, but it does not influence the finite element approximations within the element.

Finite element models based on elements with drilling freedoms at the element level inherently possess stiffness for this degree of freedom and do not exhibit rank deficiency. Several researchers use the drilling freedoms to increase the finite element approximation of the in-plane displacement field of the element (e.g., see Refs. 8–15). In this case, the drilling freedom is resisted, and a singularity or rank deficiency does not occur even for coplanar elements. These elements generally exhibit improved membrane response as well as a reduced sensitivity to element distortion.

Surface Normals

Surface normals are related to the drilling freedom issue. Here a separate nodal coordinate system, or nodal triad, is introduced at the element nodal level so that the computational degrees of freedom can be easily restrained. The nodal triad of the computational degrees of freedom for flat shell elements usually corresponds to the original nodal triad in the global coordinate system. In modeling curved surfaces with flat shell elements, each element may generate different independent nodal surface normals that are defined at shared nodes common to multiple elements, as indicated in Fig. 1. If the elements connected at a particular node happen to be coplanar, then these element surface normals are identical, and a rank deficiency exists in the assembled matrix. That is, the drilling freedom, which is not resisted, causes a singularity in the global stiffness matrix. In this case, the computational nodal freedoms are already aligned with the element nodal directions, and the drilling freedoms may be suppressed at the beginning of an analysis if the element does not support drilling freedoms. However, if the elements are not coplanar, such as in the case of the facet approximation of the curved structure shown in Fig. 1, then the element surface normals and the direction of the associated drilling freedom from each element will differ by angle β. The rank deficiency is avoided because the drilling rotation of one element is resisted by a bending stiffness from an adjacent element. This difference is generated by the faceted approximations made for the shell geometry, and the severity of this difference diminishes as the finite-element mesh is refined. That is, as the number of elements along the curved surface increases, the angle β between the surface normals of adjacent elements ($\boldsymbol{n}_1$ and $\boldsymbol{n}_2$) decreases, and a rank deficiency occurs. Typically, these element nodal normals are used to define an average nodal surface normal vector, which is then used as the outward normal direction in the computational triad for the nodal degrees of freedom. However, for more general situations, the computational triad may not be easily aligned or the rank deficiency associated with an unsupported drilling degree of freedom may not be easily eliminated, and it is necessary to treat these computational triads in a more robust fashion as described next.

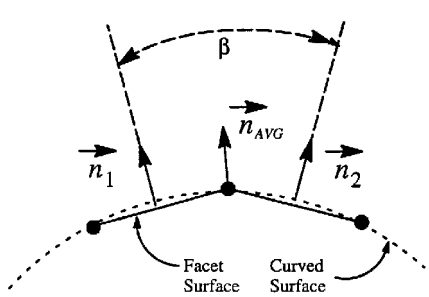

Fig. 1 Typical surface normals for two adjacent flat shell elements.

Computational Framework

To provide a nearly level playing field to assess these aspects relative to the performance of the shell elements, the NASA Langley Research Center's structural analysis software framework COMET[16] was used. This evaluation is possible through the use of COMET's generic element processor[17] feature and the commonality of other aspects of the analysis (assembler, solver, etc.). Elements included in this study are briefly summarized in Table 1 (Refs. 15, 16, and 18–22). Of the shell elements, only the 4_STG and 3_DKT elements neglect transverse shear, whereas 4_ANS, AQ4, and MIN3 account for transverse shear deformation. The AQ4 element includes the drilling freedoms in the finite-element approximations for in-plane displacement field. The MIN3 element uses a penalty approach to eliminate the drilling freedoms. Both solid elements have eight nodes; however, the 8_HYB element is an assumed-stress hybrid element, which is quite good in bending.

COMET provides three options related to drilling stiffness suppression and the realignment of shell surface normals. Users may specify parameters for automatic drilling stiffness (`auto_drill`), automatic degree-of-freedom suppression (`auto_dof_sup`), or automatic surface normal realignment (`auto_triad`). The first option is the automatic drilling stiffness option, which, if active, provides artificial drilling stiffness for those elements without drilling freedoms included in their formulation. Essentially, this option adds a diagonal contribution to the element stiffness matrix for those elements located in the structural model where the angle between the average nodal normal and the attached element normal is less than some tolerance (COMET default value is 1 deg). In such cases, the artificial drilling stiffness added to the element stiffness matrix is defined as the maximum diagonal stiffness coefficient scaled by a factor of 10^{-g}, where g has a default value of 5 in COMET. Note that these adjustments are made after transforming the nodal blocks of the element stiffness matrix for the global or element coordinate system to the local coordinate system in which the outward axis is parallel to the outward normal or drilling axis.

The second option is the automatic degree-of-freedom suppression option, which, if active, determines whether to suppress computational degrees of freedom that have insufficient stiffness. This option can be used to suppress degrees of freedom not supported by the element automatically. In this case, this option essentially eliminates those drilling degrees of freedom at nodes where the angles between the surface normal of the nodal computational triad and all element normals attached to that node are less than some tolerance (COMET default value is 1 deg). If the angle between a computational axis at a given node and any attached element normal is greater than this tolerance, then the computational drilling degree of freedom is not suppressed. If all element normals make an angle with a computational axis that is less than or equal to the tolerance, then the computational drilling degree of freedom is suppressed.

Table 1 Elements considered in this study

Element label	COMET element name	Element description	Ref.
4_ANS	ES1/EX47	Four-node, flat C^0 shell element based on the assumed natural-coordinate strain formulation	16, 18
4_STG	ES5/E410	Four-node flat C^1 shell element based on displacement formulation from STAGS	16, 19
AQ4	ES24/A4S1	Four-node flat C^0 shell element based on assumed-stress hybrid formulation and including drilling freedoms	15
4_HYB	ES4/EX43	Four-node flat C^0 shell element based on assumed-stress hybrid formulation	16, 20
MIN3	ES36/MIN3	Three-node flat C^0 shell element based on displacement formulation; automatically artificial drilling stiffness is added at every node	21
3_DKT	ES31/TP2L	Three-node flat shell element based on displacement formulation and the discrete Kirchhoff approximations	22
8_HEX	ES10/BR08	Eight-node brick element based on displacement formulation and using full integration	16
8_HYB	ES3/EX08	Eight-node brick element based on assumed-stress hybrid formulation	16, 20

This option results in generation of a homogeneous single-point constraint for those degrees of freedom similar to that of a fixed condition as a boundary condition.

The third option is the automatic surface normal realignment option, which, if active, determines whether a new coordinate system or nodal triad is to be defined at nodes when the angle between the average nodal normal and the attached element normal is less than some tolerance (the COMET default value is 1 deg). In such cases, the computational triads at all element nodes are replaced with new triads so that the local outward axis is parallel to the average nodal normal and the other axes form an orthogonal triad. Hence, the computational degrees of freedom are aligned with the unit triad system oriented as the average element normal at that node. This new triad is based on element geometry and orientation of the element in the overall structural model. With the new computational triads defined, the automatic degree-of-freedom suppression option is then invoked to possibly eliminate or constrain any unsupported drilling degrees of freedom. Degrees of freedom to be constrained or eliminated are identified and a homogeneous single-point constraint is generated similar to a fixed degree of freedom as a boundary condition.

The `auto_drill` option would normally be used without either of the other two options activated. The `auto_dof_sup` option can be used to suppress degrees of freedom not supported by the element (such as rotations for solid elements). The `auto_triad` option would normally be used in conjunction with the `auto_dof_sup` option. The `auto_triad` option examines the orientation of the element within the structural model and realigns computational triads. The `auto_dof_sup` option tests and removes any such degree of freedom. Only the latter combination of the `auto_triad` and `auto_dof_sup` options is considered in this study.

Raasch Challenge

The Raasch challenge problem grew out of a presentation at the Structures Technical Forum at the 1990 MSC World Users' Conference.[5,6] The geometry is essentially that of a "hook," as shown in Fig. 2. The hook is a thick curved strip clamped at one end (all degrees of freedom constrained to zero) and loaded by a unit in-plane shear load in the width (or z) direction at the other end. In this paper, the unit shear load is treated as a uniformly distributed shear load of 0.05 lb/in. (total shear force of 1.0 lb). The hook has essentially two different curved segments that are tangent at their point of intersection. One segment spans an opening angle of 60 deg and has a radius of 14 in. The second segment spans an opening angle of 150 deg and has a radius of 46 in. Both segments have thicknesses t of 2.0 in. and widths w of 20 in. [aspect ratio w/t equal to 10 (limit for first-order, shear-deformation theory)]. The hook material is isotropic, with an elastic modulus of 3300 psi and a Poisson ratio of 0.35.

Early MSC/NASTRAN results[5] for this problem indicated that as the mesh of QUAD4[23] elements was refined, the solution did not converge unless the transverse shear flexibility (controlled by the parameter MID3) was suppressed. Recommendations to users

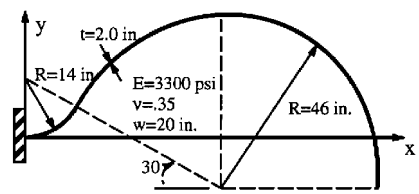

Fig. 2 Geometry of the Raasch challenge problem.

at that time were to suppress the transverse shear flexibility (set MID3 = 0 on the PSHELL card) and also to suppress the drilling freedoms caused by the facet shell geometry approximations (use a large value for the artificial stiffness parameter K6ROT). The MSC element developers then proceeded to develop the QUADR element, which included a drilling freedom at each node and also created the unique surface normal option for the low-order shell elements to resolve this behavior and to improve element performance of their low-order quadrilateral elements over that reported by MacNeal and Harder.[3]

At the 1995 MSC World Users' Conference, Hoff et al.[6] presented new results for this problem by using both the QUAD4 and QUADR shell elements from MSC/NASTRAN Version 68.2. The QUAD4 element is a four-node flat, quadrilateral, displacement-based shell element without any drilling freedoms. The QUADR element is related to the QUAD4 and includes drilling freedoms at the nodes. Both shell elements can accommodate transverse shear flexibility. These new results also indicate that, as the mesh is refined, the solution does not converge for either shell element unless transverse shear flexibility is suppressed or unique normals are used. The addition of drilling freedoms to the element formulation (i.e., the QUADR element) did provide some improvement in the element performance, but the solutions obtained with successively refined meshes still did not converge. The value of the tip deflection in the direction of the load obtained for the most refined mesh using the QUADR element was still more than twice their reported converged value (given as 5.012 in. in Ref. 6) and represents an improvement over the value obtained with the QUAD4 element, which was nearly five times the converged value. Results also were presented with a new surface normal option (SNORM parameter) that activates the creation of unique grid point normals for adjacent shell elements.[6] Details of this option are not presented. With surface normals active and transverse shear flexibility suppressed, the solutions obtained without and with nodal drilling freedoms (QUAD4 and QUADR elements, respectively) are essentially the same and exhibit rapid convergence. In addition, the solutions obtained with surface normals active and with transverse shear flexibility included converge rapidly to their reference solution for both elements, which corresponds to a value approximately 5% more flexible than that obtained with transverse shear flexibility suppressed. Hoff et al.[6] concluded that unique surface normals at grid points are needed to improve the element performance of the MSC low-order quadrilaterals.

Numerical Results

Various numerical studies were performed to assess the performance of the elements shown in Table 1 and considered in this study. Included in this assessment were the original MacNeal–Harder test cases,[3] and all of the elements performed quite well for cases involving regular rectangular meshes. These tests include the cantilever straight, curved, and twisted beams with in-plane shear, out-of-plane bending, and torsion loads. The performance of some elements deteriorated when element distortion occurred (e.g., see Ref. 15). Here only two geometries are considered: a flattened hook and the original Raasch hook. In all cases, regular meshes of rectangular or brick-shaped elements are considered, and element distortion is not an issue. The boundary conditions imposed at the clamped end have all degrees of freedom constrained to zero. Results are first presented for a straight-beam problem (flattened hook) and then for the Raasch challenge problem (curved hook).

Straight Cantilever Beam (Flattened Hook)

The capability of the element to handle constant and linearly varying strains and curvatures is tested by applying appropriate unit loads at the free end. The straight beam (or flattened hook) geometry considered here is selected to be similar to the curved hook problem—that is, a flattened hook where the length of the straight beam is equal to the total arc length of the hook. The clamped boundary conditions restrain all degrees of freedom along that boundary for the two-dimensional shell elements. For the three-dimensional solid elements, the model is free to expand in the thickness direction, which is consistent with two-dimensional theory. The tip loading condition corresponds to an in-plane shear load of unit magnitude in the z direction along the beam width.

Various finite element models are considered including both two- and three-dimensional models. The mesh is defined as the number of elements in the width direction n_w by the number of elements along the beam length n_L; that is, $n_w \times n_L$. The three-dimensional models have two elements through the thickness of the beam. The nodes are distributed equally in each of the directions. Normalized results for various spatial discretizations are given in Table 2. These results indicate that a converged solution is obtained for each element type as the mesh is successively refined. However, this loading condition does not cause any coupling between the membrane and bending approximations in the element, and the problem is simply a plane stress problem with no out-of-plane deformations. In addition, the extension and out-of-plane bending loading cases are considered, and the results, although not shown here, are similar to those given in Table 2.

Raasch Challenge (Curved Hook)

Different forms of the hook problem have been considered (see Ref. 5); however, the more common geometry is that defined by Ingo Raasch and shown in Fig. 2. This problem poses a significant challenge to shell elements because of the inherent coupling between three modes of deformation: bending, extension, and twist. Various finite element models are considered in this study including both two- and three-dimensional models as indicated in Fig. 3. The mesh is again defined as the number of elements in the width direction n_w

Table 2 Flat straight cantilever beam results for in-plane shear loading[a]

Mesh of elements	Normalized tip deflection in direction of load					
$n_w \times n_L$	4_ANS	4_STG	AQ4	4_HYB	8_HEX	8_HYB
1×9	0.8771	1.3776	0.9974	0.9974	0.7365	0.9971
3×17	0.9806	1.0038	0.9974	0.9959	0.9243	0.9951
5×34	0.9927	1.0038	0.9990	0.9985	0.9767	0.9982
10×68	0.9985	1.0006	1.0001	0.9996	0.9938	0.9995
20×136	0.9996	1.0001	1.0001	1.0001	0.9984	1.0000

[a]Results are normalized by a solution obtained by using a $20 \times 136 \times 2$ mesh of eight-node, assumed-stress hybrid brick elements (8_HYB): 0.18938 in.

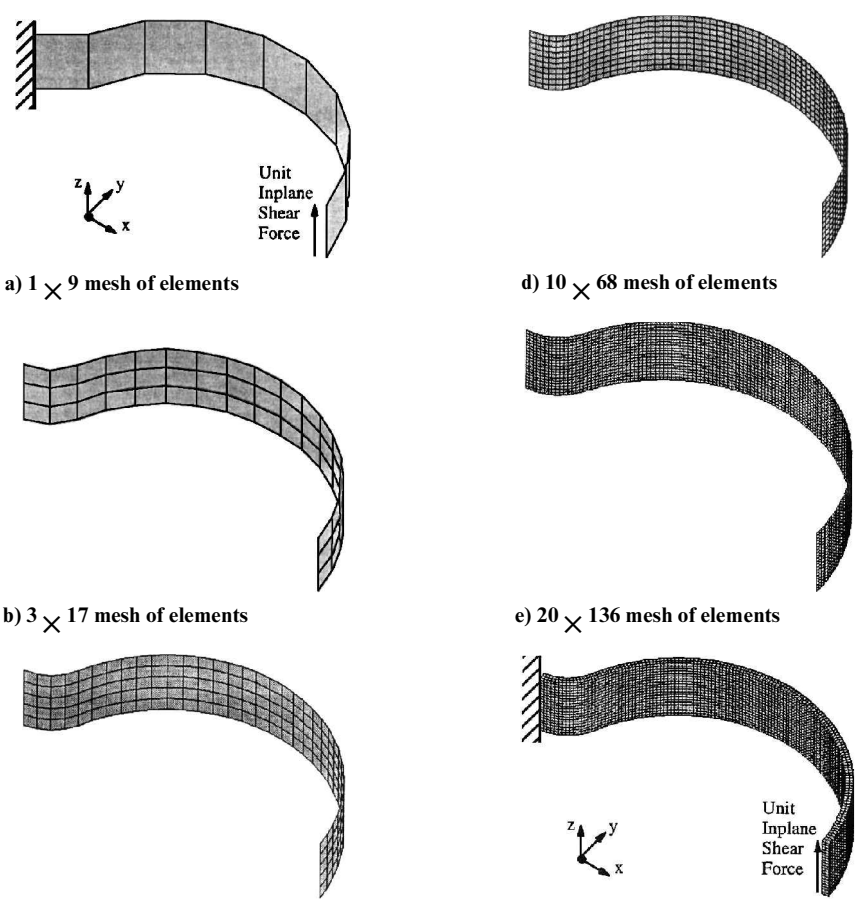

Fig. 3 Two-dimensional four-node shell quadrilateral finite element models considered and three-dimensional eight-node brick finite element model used as reference solution.

Table 3 Curved hook results for in-plane shear loading[a]

Mesh of elements $n_w \times n_L$	Normalized tip deflection in direction of load							
	4_ANS	4_STG	AQ4	4_HYB	MIN3	3_DKT	8_HEX	8_HYB
1×9	0.9411	0.9061	1.1382	1.1562	1.0666	0.8481	0.5041	0.6922
3×17	1.0335	0.9398	1.0375	1.1678	1.1341	0.9323	0.8136	0.9432
5×34	1.2559	0.9512	1.1064	1.3858	1.2588	0.9478	0.9275	0.9738
10×68	2.0618	0.9541	1.3492	2.1767	1.6357	0.9532	0.9736	0.9890
20×136	4.8111	0.9548	2.2529	4.9045	2.7760	0.9479	0.9932	1.0000

[a]Results are normalized by a solution obtained by using a $20 \times 136 \times 2$ mesh of eight-node, assumed-stress hybrid solid brick elements (8_HYB): 4.9352 for $w/t = 10$; `auto_dof_sup = true; auto_triad = false`.

by the number of elements along the hook length n_L; that is, $n_w \times n_L$. Meshes involving triangular elements are developed by subdividing each quadrilateral element into two triangular elements. Three-dimensional models have only two elements through the thickness of the hook. The nodes are distributed equally in each direction. The unit in-plane shear load is considered as a uniformly distributed traction, and work-equivalent consistent nodal loads are computed at the element level. For the three-dimensional models, the clamped boundary is fully constrained rather than allowing for through-the-thickness expansion. Results from both boundary condition cases using the most refined three-dimensional model indicate that the tip deflection is 4.9352 in. when fully constrained and 4.9366 in. when expansion in the thickness direction is permitted.

The results for various spatial discretizations and different shell elements are given in Table 3, where the isotropic properties of the material are used—that is, the transverse shear moduli are equal to the in-plane shear modulus [i.e., $G_{13} = G_{23} = G_{12} = E/2(1+\nu)$]. The reference value for the tip deflection used here is 4.9352 in. obtained with a refined $20 \times 136 \times 2$ mesh of eight-node, assumed-stress hybrid solid brick elements (8_HYB). This value represents a solution 1.6% stiffer than that given in Ref. 6. In all shell element models, the `auto_dof_sup` option is true, and the option `auto_triad` is false. The shell elements that neglect transverse shear flexibilities (4_STG, 3_DKT) converge to a solution that is slightly stiffer than the solution obtained by using a refined mesh of three-dimensional solid elements. This behavior indicates that transverse shear flexibilities at most can account for only 5% of the tip deflection. However, the solutions obtained with elements that do account for transverse shear flexibilities do not converge as the mesh is refined. The MIN3 and AQ4 elements give somewhat better solutions than the 4_ANS and 4_HYB elements but still predict more than twice the tip deflection of the three-dimensional solution for the most refined mesh. The MIN3 element suppresses all drilling freedoms at the element level (artificial drilling stiffness), whereas the AQ4 element includes the drilling freedoms to improve the in-plane displacement field approximations. By including the drilling freedoms, the approximation for the in-plane displacement field component normal to an element edge is raised from linear to quadratic along that edge.

To investigate the influence of transverse shear flexibility, two studies were performed. First, a transverse shear stiffness penalty parameter f is introduced. The effect of changing the transverse shear stiffness penalty on the solution obtained with the AQ4 quadrilateral element is shown in Table 4. Here the transverse shear moduli are set equal to a scaled value of the in-plane shear modulus [i.e., $G_{13} = G_{23} = fG_{12} = fE/2(1+\nu)$]. The normalized tip deflections obtained for $f = 1$ correspond to those given in Table 3. As the value of f increases, the effect of transverse shear flexibility decreases and is essentially fully suppressed when the penalty parameter reaches a value of 10^6. The solution obtained with the AQ4 shell element appears to be slowly converging to a solution 10% more flexible than the three-dimensional solution. Sensitivity of the solution to values of the penalty parameter disappears above values equal to 10,000.

Results obtained with the shear-flexible elements in Table 1 with high values of the transverse shear stiffness (i.e., $f = 10^6$) are given in Table 5. The results obtained with the 4_ANS element converge to the solution obtained by those elements without transverse shear flexibility. However, the AQ4, MIN3, and 4_HYB predict tip deflections that are more flexible than the three-dimensional solutions.

Table 4 Effect of various values of transverse shear stiffnesses on tip deflection[a]

Mesh of elements $n_w \times n_L$	Normalized tip deflection in direction of load			
	$f = 1$	$f = 100$	$f = 10{,}000$	$f = 10^6$
1×9	1.1382	1.1229	1.1228	1.1228
3×17	1.0375	1.0118	1.0115	1.0115
5×34	1.1064	1.0367	1.0358	1.0358
10×68	1.3492	1.0716	1.0668	1.0668
20×136	2.2529	1.1241	1.0966	1.0963

[a]Results are normalized by a solution obtained by using a $20 \times 136 \times 2$ mesh of eight-node, assumed-stress hybrid solid brick elements (8_HYB): 4.9352 for $w/t = 10$; `auto_dof_sup = true`; `auto_triad = false`; scale factor for transverse shear stiffnesses, $G_{13} = G_{23} = fG_{12}$; element type AQ4.

Table 5 Effect of high transverse shear stiffness penalty on tip deflection[a]

Mesh of elements $n_w \times n_L$	Normalized tip deflection in direction of load			
	4_ANS	AQ4	4_HYB	MIN3
1×9	0.9121	1.1228	1.1259	1.0554
3×17	0.9447	1.0115	1.0761	1.0915
5×34	0.9523	1.0358	1.0809	1.1158
10×68	0.9544	1.0668	1.0744	1.0996
20×136	0.9549	1.0963	1.0584	1.0288

[a]Results are normalized by a solution obtained by using a $20 \times 136 \times 2$ mesh of eight-node, assumed-stress hybrid solid brick elements (8_HYB): 4.9352 for $w/t = 10$; `auto_dof_sup = true`; `auto_triad = false`.

To further investigate this behavior, the thickness of the hook is decreased in two steps rather than by using a penalty parameter on the transverse shear moduli. The ratio of the hook width w to the hook thickness t is originally equal to 10. Results are given in Table 6 for values of this ratio equal to 10, 100, and 1000 to simulate a very thin hook. These results indicate that the 4_STG element, which neglects transverse shear flexibility, converges from below to the three-dimensional solution as w/t increases. Results for the AQ4 element appear to be converging to the three-dimensional solution from above. In both cases, the tip deflection obtained for a value of $w/t = 1000$ is still approximately 2% too flexible but in good agreement with the results obtained with the 4_STG element.

Next, the influence of two options to control the drilling stiffness are considered. One is the automatic degree-of-freedom suppression (`auto_dof_sup`) option, and the other is the automatic realignment of surface normals (`auto_triad`) option. The effect of these options on the constraints imposed on the finite-element model is indicated in Fig. 4, which shows the constrained degrees of freedom for the 5×34 element model (see Fig. 4a). In Fig. 4b, only the constrained degrees of freedom at the clamped boundary are imposed because both `auto_dof_sup` and `auto_triad` are inactive. In Fig. 4c, the constrained degrees of freedom also include the drilling rotations (double-headed arrows) at the hook tip because `auto_dof_sup` is active but `auto_triad` is inactive. In Fig. 4d, all rotations normal to the hook surface are constrained because both `auto_dof_sup` and `auto_triad` are active.

These options affect the performance of the 4_ANS and AQ4 shell elements, as indicated in Table 7, where a tolerance of 15 deg is used for the angle between the average nodal normal and the element nodal normal. This value is selected so that the drilling freedom

Table 6 Effect of various width-to-thickness aspect ratios on tip deflection[a]

Mesh of elements $n_w \times n_L$	Normalized tip deflection in direction of load					
	Element type AQ4			Element type 4_STG		
	$w/t = 10$	$w/t = 100$	$w/t = 1000$	$w/t = 10$	$w/t = 100$	$w/t = 1000$
1 × 9	1.1382	1.1605	1.1780	0.9061	0.9448	0.9593
3 × 17	1.0375	1.0250	1.0406	0.9398	0.9837	0.9988
5 × 34	1.1064	1.0212	1.0332	0.9512	0.9957	1.0104
10 × 68	1.3492	1.0207	1.0249	0.9541	0.9988	1.0136
20 × 136	2.2529	1.0350	1.0205	0.9548	0.9996	1.0145

[a]Results for each aspect ratio are normalized by a solution obtained by using a 20 × 136 × 2 mesh of eight-node, assumed-stress hybrid solid brick elements (8_HYB): 4.9352 for $w/t = 10$; 4659.984 for $w/t = 100$; and 45,886,787 for $w/t = 1000$. `auto_dof_sup = true`; `auto_triad = false`.

Table 7 Effect of surface normals on tip deflections

Mesh of elements $n_w \times n_L$	Normalized tip deflection in direction of load					
	4_ANS element			AQ4 element[a]		
	`auto_dof_sup = false` `auto_triad = false`	`auto_dof_sup = true` `auto_triad = false`	`auto_dof_sup = true` `auto_triad = true`	`auto_dof_sup = false` `auto_triad = false`	`auto_dof_sup = true` `auto_triad = false`	`auto_dof_sup = true` `auto_triad = true`
1 × 9	0.9411	0.9411	0.0529	1.1382	1.1382	0.1345
3 × 17	1.0335	1.0335	0.1549	1.0375	1.0375	0.2203
5 × 34	1.2559	1.2559	0.4561	1.1064	1.1064	0.4589
10 × 68	2.0618	2.0618	0.9572	1.3492	1.3492	0.8680
20 × 136	4.8111	4.8111	1.3502	2.2529	2.2529	1.2841

[a]AQ4 results with `auto_dof_sup = true` and `auto_triad = true` are for the case with all rotations normal to the hook surface suppressed.

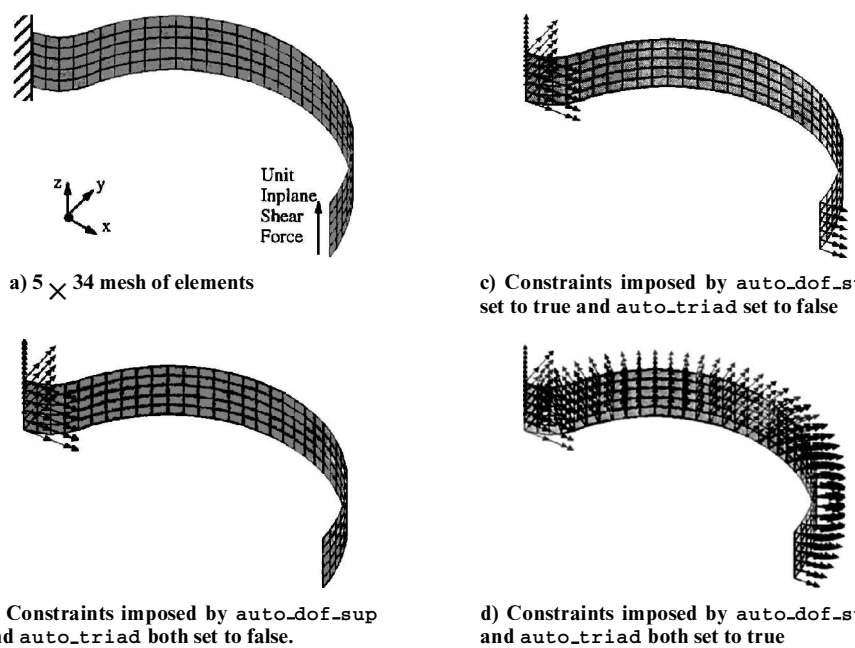

a) 5 × 34 mesh of elements

c) Constraints imposed by `auto_dof_sup` set to true and `auto_triad` set to false

b) Constraints imposed by `auto_dof_sup` and `auto_triad` both set to false.

d) Constraints imposed by `auto_dof_sup` and `auto_triad` both set to true

Fig. 4 Constraints imposed of the 5 × 34 quadrilateral shell element model using different options to suppress drilling freedoms.

suppression patterns shown in Fig. 4 are obtained for all meshes considered. When `auto_triad` is inactive (or false), essentially no difference in results occurs for either value of `auto_dof_sup`, because the equation solver in COMET automatically detects initial zeroes in the stiffness matrix and removes them before matrix decomposition for the case when `auto_dof_sup` is inactive. When `auto_triad` is active (or true), all nodal triads are realigned to be normal to the hook surface so that normal rotations can be easily suppressed. This should correspond to the MSC case with unique surface normals active. For the 4_ANS element, the results approach the three-dimensional solution from below but still do not indicate a converging behavior. The AQ4 element has a drilling freedom, and suppression of the rotations normal to the hook surface should not be done because it is included in the element formulation. Hence, the data for each column in Table 7 are identical for the AQ4 element. However, by forcing the drilling freedoms to be constrained for this element, results similar to the 4_ANS element are obtained.

Summary

This paper examines the Raasch challenge problem in an attempt to better understand how certain shell element features affect the solution. Shell elements without transverse shear flexibility in COMET (4_STG and 3_DKT) appear to converge to an appropriate value (i.e., 5% stiffer than the three-dimensional solution). Shell elements with transverse shear flexibility do not appear to converge. Surface normals or new computational nodal triads influence the results obtained with COMET but not as successfully as reported by Hoff et al.[6] If the hook is made thin, then all shell elements tested converge.

Shell finite-element development should continue to be an active area of research. Anomalies and pathological problems associated with many shell elements still remain. The intelligent use of the elements and thorough examination of the models and their predictions continues to be a major contributor to a successful finite-element analysis. The need for increased reliability in our computed

solutions will continue to grow as the reliance on analytical results increases for systems where verification by experiment is not feasible, economical, or timely.

Acknowledgments

The research was sponsored by the NASA Langley Research Center under NASA Grant NAG-1-1505 with Alexander Tessler as the contracting officer's technical representative. The author also gratefully acknowledges the contributions of Tina Lotts of Analytical Services and Materials, Inc.

References

[1]Taylor, R. L., "Finite Element Analysis of Linear Shell Problems," *The Mathematics of Finite Elements and Applications VI—MAFELAP 1987*, edited by J. R. Whiteman, Academic, New York, 1988, pp. 191–203.

[2]Noor, A. K., Belytschko, T., and Simo, J. C. (eds.), *Analytical and Computational Models of Shells*, Vol. 3, American Society of Mechanical Engineers, New York, 1989.

[3]MacNeal, R. H., and Harder, R. L., "A Proposed Standard Set of Problems to Test Finite Element Accuracy," *Finite Elements in Analysis and Design*, Vol. 1, No. 1, 1985, pp. 3–20.

[4]Belytschko, T., and Liu, W. K., "Test Problems and Anomalies in Shell Finite Elements," *Reliability of Methods for Engineering Analysis*, edited by K. J. Bathe and D. R. J. Owen, Pineridge, Swansea, Wales, UK, 1986, pp. 393–406.

[5]Harder, R. L., "The Raasch Challenge," Presentation charts presented at the Structures Technical Forum at the 1991 MSC World Users' Conference (12 charts), Los Angeles, CA, 1991.

[6]Hoff, C. C., Harder, R. L., Campbell, G., MacNeal, R. H., and Wilson, C. T., "Analysis of Shell Structures using MSC/NASTRAN's Shell Elements with Surface Normals," *Proceedings of the 1995 MSC World Users' Conference* (Universal City, CA), MacNeal–Schwendler Corp., Paper 26, Los Angeles, CA, 1995, 18 pp.

[7]Belytschko, T., "Linear Finite Elements—Have All the Problems Been Solved?," *USACM Newsletter*, Vol. 1, No. 3, 1988, pp. 2, 3.

[8]Allman, D. J., "A Compatible Triangular Element Including Vertex Rotations for Plane Elasticity Analysis," *Computers and Structures*, Vol. 19, No. 1–2, 1984, pp. 1–8.

[9]Bergan, P. A., and Felippa, C. A., "A Triangular Element with Rotational Degrees of Freedom," *Computer Methods in Applied Mechanics and Engineering*, Vol. 50, No. 1, 1985, pp. 25–69.

[10]Ibrahimbegovic, A., Taylor, R. L., and Wilson, E. L., "A Robust Quadrilateral Membrane Finite Element with Drilling Degrees of Freedom," *International Journal for Numerical Methods in Engineering*, Vol. 30, No. 3, 1990, pp. 445–457.

[11]Ibrahimbegovic, A., and Wilson, E. L., "A Unified Formulation for Triangular and Quadrilateral Flat Shell Finite Elements with Six Nodal Degrees of Freedom," *Communications in Applied Numerical Methods*, Vol. 7, No. 1, 1991, pp. 1–9.

[12]Iura, M., and Atluri, S. N., "Formulation of a Membrane Finite Element with Drilling Degrees of Freedom," *Computational Mechanics*, Vol. 9, No. 6, 1992, pp. 417–428.

[13]MacNeal, R. H., and Harder, R. L., "A Refined Four-Noded Membrane Element with Rotational Degrees of Freedom," *Computers and Structures*, Vol. 28, No. 1, 1988, pp. 75–84.

[14]Yunus, S. H., Saigal, S., and Cook, R. D., "On Improved Hybrid Finite Elements with Rotational Degrees of Freedom," *International Journal for Numerical Methods in Engineering*, Vol. 28, No. 4, 1989, pp. 785–800.

[15]Rengarajan, G., Aminpour, M. A., and Knight, N. F., Jr., "Improved Assumed-Stress Hybrid Shell Element with Drilling Degrees of Freedom for Linear Stress, Buckling, and Free Vibration Analyses," *International Journal for Numerical Methods in Engineering*, Vol. 38, No. 11, 1995, pp. 1917–1943.

[16]Stewart, C. B. (compiler), "The Computational Structural Mechanics Testbed Users' Manual," NASA TM-100644 (updated), 1990.

[17]Stanley, G. M., and Nour-Omid, S., "The Computational Structural Mechanics Testbed Generic Structural Element Processor Manual," NASA CR-181728, 1990.

[18]Stanley, G. M., "The Computational Structural Mechanics Testbed Structural Element Processor ES1: Basic SRI and ANS Elements," NASA CR-4357, 1991.

[19]Rankin, C. C., and Brogan, F. A., "The Computational Structural Mechanics Testbed Structural Element Processor ES5: STAGS Shell Element," NASA CR-4358, 1991.

[20]Aminpour, M. A., "Assessment of SPAR Elements and Formulation of Some Basic 2-D and 3-D Elements for Use with Testbed Generic Element Processor," *Proceedings of NASA Workshop on Computational Structural Mechanics*, edited by N. P. Sykes, NASA CP-10012, Pt. 2, 1989, pp. 653–682.

[21]Tessler, A., and Hughes, T. J. R., "A Three-Node Mindlin Plate Element with Improved Transverse Shear," *Computer Methods in Applied Mechanics and Engineering*, Vol. 50, No. 1, 1985, pp. 71–101.

[22]Garnet, H., and Pifko, A., "An Efficient Triangular Plate Bending Finite Element for Crash Simulation," *Computers and Structures*, Vol. 16, Nos. 1–4, 1983, pp. 371–379.

[23]MacNeal, R. H., "A Simple Quadrilateral Shell Element," *Computers and Structures*, Vol. 8, No. 2, 1978, pp. 175–183.